

Mechanisms of aerosol-forced AMOC variability in a state of the art climate model

Matthew B. Menary,¹ Christopher D. Roberts,¹ Matthew D. Palmer,¹ Paul R. Halloran,¹ Laura Jackson,¹ Richard A. Wood,¹ Wolfgang A. Müller,² Daniela Matei,² and Sang-Ki Lee³

Received 29 October 2012; revised 21 March 2013; accepted 25 March 2013; published 25 April 2013.

[1] Mechanisms of sustained multidecadal changes in the strength of the Atlantic Meridional Overturning Circulation (AMOC) are investigated in a set of simulations with a new state-of-the-art Earth system model. Anthropogenic aerosols have previously been highlighted as a potential mitigator of AMOC weakening. In this study, we explain the oceanic mechanisms behind how anthropogenic aerosols force a strengthening of the AMOC by up to 20% in our state-of-the-art Earth system model. This strengthening is driven via atmospheric circulation changes which subsequently modulate the salinity budget of the North Atlantic subpolar gyre. Gradual salinification occurs via increased evaporation and decreased fluxes of ice through the Fram Straits. A component of the salinification is a positive feedback from the AMOC bringing more saline water northwards from the subtropical Atlantic. Salinification of the subpolar gyre results in increased deep convection and a strengthening of the AMOC. Following a reduction in aerosol concentrations, the AMOC rapidly weakens, approximately 3 times faster than in the case where anthropogenic aerosol concentrations had never been increased. Similarities and differences with available observational records and long term reanalysis products are also discussed.

Citation: Menary, M. B., C. D. Roberts, M. D. Palmer, P. R. Halloran, L. Jackson, R. A. Wood, W. A. Müller, D. Matei, and S.-K. Lee (2013), Mechanisms of aerosol-forced AMOC variability in a state of the art climate model, *J. Geophys. Res. Oceans*, 118, 2087–2096, doi:10.1002/jgrc.20178.

1. Introduction

[2] Through its northward heat transport (~1.3 PW at 25°N) [Johns *et al.*, 2011], the Atlantic Meridional Overturning Circulation (AMOC) is believed to have a considerable impact on the mean state and variability of climate in the North Atlantic region [Latif and Keenlyside, 2011; Minobe *et al.*, 2008; Zhang and Delworth, 2005]. Palaeoclimate evidence suggests past abrupt climate changes are linked to variability in the AMOC [McManus *et al.*, 2004], whereas modeling studies suggest that a collapse of the AMOC could result in regional surface temperature changes as large as 8°C [Vellinga and Wood, 2002]. The magnitude of a simulated AMOC response to external forcing may also be related to the absolute strength of the AMOC simulated during a preindustrial climate [Gregory *et al.*, 2005], though this may also depend on the representation of the external forcing (e.g., greenhouse gases (GHGs) or freshwater hosing) [Clark *et al.*, 2002; Stouffer *et al.*, 2006]. The response of the AMOC to estimates

of historical and future radiative forcings has been widely studied using the previous generation of coupled climate models [Meehl *et al.*, 2007; Schmittner *et al.*, 2005]. These studies have led to the current paradigm of little change in the AMOC over the twentieth century due to external forcings, with weakening expected from the late twentieth or early 21st century associated with GHG warming and changes to surface heat fluxes [Gregory *et al.*, 2005]. However, a number of recent studies suggest that GHG forcing is not the only external forcing of relevance for the response of ocean circulation. A model study by Delworth and Dixon [2006] showed no AMOC weakening during the twentieth century as aerosol forced cooling (and salinification from associated hydrological cycle changes) of the subpolar gyre (SPG) compensated for the warming and freshening due to increasing GHGs. Cai *et al.* [2006] also found that AMOC weakening can be mitigated by aerosol forcing, though detailed analyses of the oceanic mechanisms were not presented.

[3] In this study, we examine the role of the atmospheric response to aerosol forcing in affecting the downstream response of the large-scale ocean circulation. After a brief description of the model and simulations used in the main analysis (section 2), we present the key result of a simulated historically strengthening AMOC (section 3.1). The mechanisms behind this response are subsequently investigated in the framework of the externally forced simulations and a preindustrial control simulation (section 3.2). We finish with a discussion of various lines of observation-based evidence

¹Met Office Hadley Centre, Met Office, Exeter, Devon, UK.

²Max Planck Institute for Meteorology, Hamburg, Germany.

³Cooperative Institute for Marine and Atmospheric Studies, University of Miami, Miami, Florida, USA.

Corresponding author: M. B. Menary, Met Office Hadley Centre, Met Office, Exeter, Devon EX1 3PB, UK. (matthew.menary@metoffice.gov.uk)

©2013. American Geophysical Union. All Rights Reserved.
2169-9275/13/10.1002/jgrc.20178

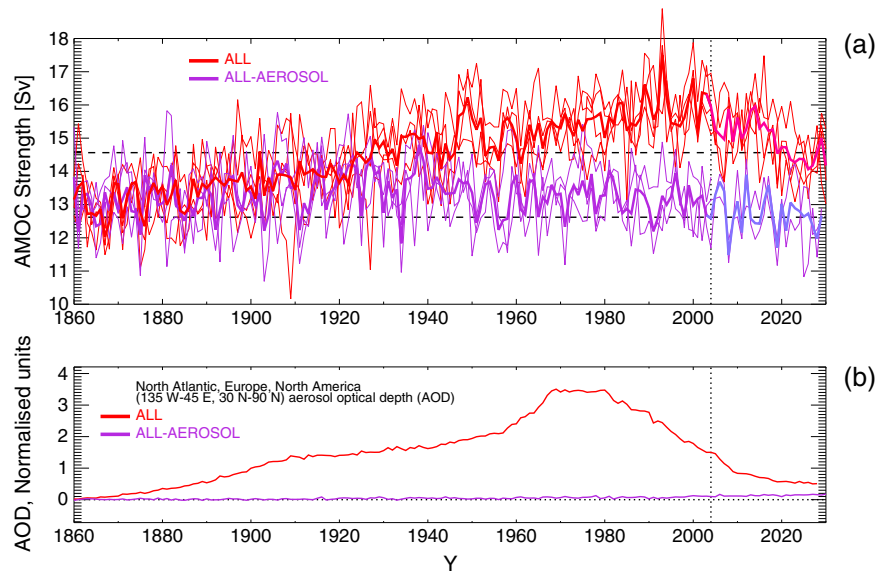


Figure 1. (a) Annual mean AMOC strengths at 30°N in HadGEM2-ES ALL (red) and ALL-AEROSOL (purple) ensembles. Plotted are the individual ensemble members (thin) and the ensemble mean (thick). From 2004, ensembles are continued until 2030 using RCP4.5 (slight change in shading). Dashed lines show the preindustrial control run mean ± 1 standard deviation range of annual mean strengths. (b) Normalized Northern Hemisphere minus Asia total aerosol optical depth anomaly (relative to 1860) in ALL (red) and ALL-AEROSOL (purple).

and compare these to our forced simulations (section 4.1) before speculating on the potential effects of future reductions in aerosol concentrations (section 4.2). Conclusions are presented in section 5.

2. Model Description

[4] Using the state-of-the-art climate model HadGEM2-ES (Hadley Centre Global Environment Model 2, with Earth System components), we have undertaken simulations of the climate over the past 150 years. The model is a coupled atmosphere, ocean, sea ice, and land surface model. The version of HadGEM2-ES used in this analysis has an ocean resolution of 1° , rising to $1/3^{\circ}$ (in latitude) near the equator and has 40 z -coordinate vertical levels. The atmospheric resolution is $1.25^{\circ} \times 1.875^{\circ}$ with 38 vertical levels. HadGEM2-ES includes a significant improvement in the scope of atmospheric, land surface, and ocean biogeochemical interactions compared to its predecessors [Collins *et al.*, 2011]. It includes complex parameterizations of ocean and land ecosystems, tropospheric chemistry, aerosols, and dynamic vegetation. The direct (radiation scattering) and first and second indirect effects (cloud brightness and cloud lifetime) of aerosols are included, as well as coupling between aerosols, chemistry, ecosystems, and climate. For a fuller description of the model and simulations, see Jones *et al.* [2011] and references therein. We use results from a 500 year long preindustrial control simulation and two initial condition ensembles with time varying external forcings. The control simulation uses climatological external forcings appropriate for the year 1860 [Jones *et al.*, 2011] and exhibits no drift in the strength of the AMOC (that is, the trend in annual mean AMOC strength is not significantly different from zero at the 95% level for a two-tailed t test). Here and throughout the AMOC is defined as the maximum of the Atlantic

overtaking streamfunction at 30°N . Each pair of initial condition ensemble members is initialized from a different point in the long control run, at intervals of 50 years, in order to sample internal variability. The forcing scenarios we have analyzed are referred to as ALL (which includes greenhouse gases, solar variability, volcanic aerosols, land use changes, and anthropogenic aerosols) and ALL-AERO (as ALL but with anthropogenic aerosol emissions held at 1860 levels). There are four members in the ALL ensemble and three members completed in the ALL-AERO ensemble. Simulations continued beyond 2005 use the representative concentration pathways (RCPs, e.g., RCP4.5) [Moss *et al.*, 2010] set out by the Intergovernmental Panel on Climate Change (IPCC). The number 4.5 represents the net Top of Atmosphere (TOA) radiative forcing, in W/m^2 , at year 2100. With the exception of aerosol concentrations, the future forcings used in ALL and ALL-AERO are identical. Results shown from ALL and ALL-AERO ensembles are ensemble means unless otherwise stated.

3. Results

3.1. AMOC Strengthening

[5] The preindustrial control simulation has a mean AMOC strength of 13.6 ± 1.0 Sverdrups (mean and 1 standard deviation of annual mean data; Sv: 1 Sverdrup = $1 \times 10^6 \text{ m}^3 \text{ s}^{-1}$). The ALL simulations show a 20% increase in the strength of the AMOC from an initial value of ~ 13 Sv to peak values of ~ 16 Sv in 1990–2000 (Figure 1a), within 1 standard deviation of the 2004–2011 annual mean AMOC strength documented by the RAPID observations [Kanzow *et al.*, 2010] of $\sim 17.5 \pm 2.3$ Sv (using the latest data from <http://www.noc.soton.ac.uk/rapidmoc/>). The AMOC strength in the preindustrial control simulation is weak compared to the RAPID observations; however, the values toward the end of

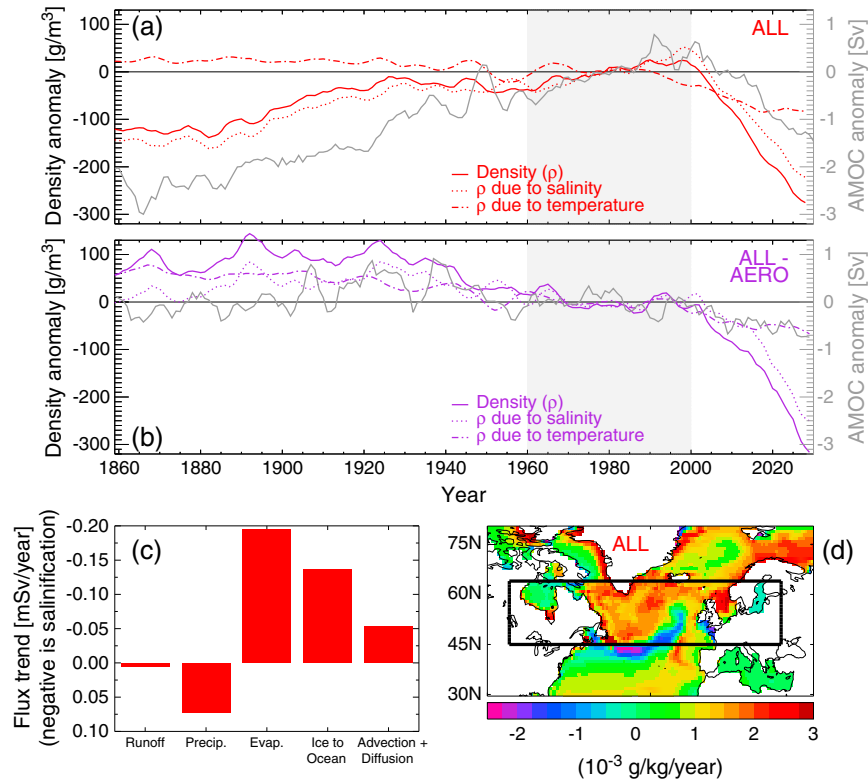


Figure 2. (a) ALL and (b) ALL-AEROSOL density anomalies relative to the period 1960–2000 (shaded), averaged over the North Atlantic SPG top 800 m: solid, total density; dotted, density due to salinity variations (evaluated using time mean temperature); dot-dashed, density due to temperature variations (evaluated using time mean salinity). Also plotted on both panels is the ensemble mean AMOC from the ensembles (right-hand axis, gray). (c) Trends in freshwater budget components for the SPG top 800 m from 1859 to 1970 in ALL. (d) Spatial map of the trend in salinity averaged over the top 800 m in ALL from 1859 to 1970.

the ALL simulation compare well to the present-day observations. The positive trend in ALL is robust across the ensemble members (thin lines on Figure 1a) and is significantly different from the internal climate variability after 1935. Trend significance in the AMOC in ALL and ALL-AERO was evaluated using the following bootstrapping approach. A pseudoensemble of four members was made using the control integration for time periods of between 2 and 100 years. This was done 10,000 times using random sections from the control to estimate the frequency of AMOC trends in an unforced simulation as a function of trend period. These distributions were then compared to the trends in the ALL and ALL-AERO ensembles and the time found at which these ensembles fell in the tails of the distribution (top or bottom 2.5% corresponding to the 95% confidence level). Beginning the trend at 1859 resulted in a significant trend detected in ALL by 1935 but no significant trend detected in ALL-AERO.

[6] Since the only difference between the ALL and ALL-AERO ensembles is the inclusion/exclusion of anthropogenic aerosols, the difference in AMOC behavior must be attributable to these changes. Normalized aerosol optical depths for a subregion of the Northern Hemisphere give an indication of the historical aerosol loading in the model simulations (Figure 1b). In contrast to ALL, the ALL-AERO simulations show no significant change in the AMOC during the historical period

[7] Unlike previous model studies [Cai *et al.*, 2006; Delworth and Dixon, 2006], the AMOC in the ALL-forcings run of HadGEM2-ES shows a persistent increase in strength, i.e., aerosol forcing does more than merely mitigate a decline. We also show in the following section that mechanisms not described previously are responsible for this increase in AMOC strength.

3.2. Mechanisms

[8] The increase in the AMOC seen in ALL is associated with an increase in the density of the upper water column (0–800 m) in the model sinking regions of the North Atlantic and particularly the SPG (defined as the range 45°N to 65°N in the Atlantic; Figure 2a). Densities in this region have been shown in a number of model studies to be closely linked to AMOC change on interdecadal time scales [e.g., Thorpe *et al.*, 2001]. The increased density acts to destabilize the water column, enhancing winter-time convection and deep-water formation rates, and ultimately leading to a stronger AMOC. By the year 2000, the trend in density in ALL has begun to reverse due to a warming of the water column, and we see a corresponding weakening of the AMOC.

[9] In ALL, the increase in density of the SPG is dominated by long-term changes in salinity. Salinity changes appear to lead AMOC changes by 0–20 years in ALL but the long-term trends in the time series make this relationship

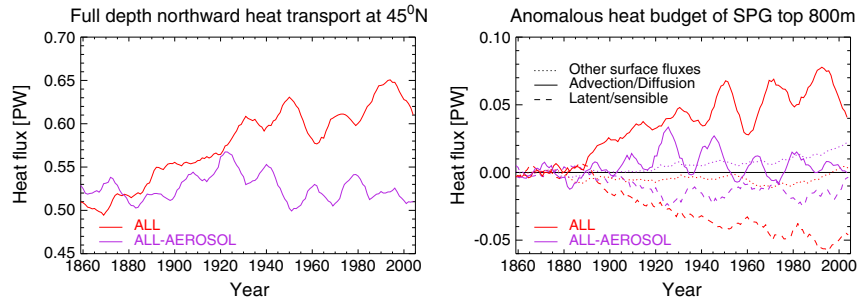


Figure 3. (a) Ensemble mean full depth northward heat transport across 45°N in ALL (red) and ALL-AEROSOL (purple), and (b) anomalous heat fluxes into the top 800 m of the SPG (45°N–65°N).

difficult to evaluate. Analysis from the control simulation reveals the AMOC lags salinity-controlled density changes in the SPG by around 10 years (not shown) in the absence of external forcings. Similar results are obtained when using a meridional density difference between the SPG and South Atlantic following *Thorpe et al.* [2001]. Additionally, it should be noted that the relationship between the AMOC and density is weakest in the centre of the SPG and strongest at the gyre boundaries, near the coasts, and in the Labrador Sea, but we have used this broader region in order to allow a more accurate calculation of the budget. By comparison, in ALL-AERO the density decreases slightly, driven in part by the warming when the historically increasing aerosol forcing is absent (Figure 2b). In ALL, as well as the increased northward heat transport associated with the AMOC (Figure 3, left), there is a compensating increase in latent and sensible heat loss (Figure 3, right), resulting in similar warming in the SPG in both ALL and ALL-AERO. A freshwater budget analysis of the SPG in ALL (Figure 2c) for the period of maximum change in SPG surface salinities (1860–1970) shows there are three primary mechanisms driving the salinification of the SPG (Figure 2d): (i) increased evaporation over the SPG, (ii) a decrease in the freshwater contribution from sea ice melt, and (iii) an increase in salt advection by the overturning circulation. Mechanisms (i) and (ii) can be

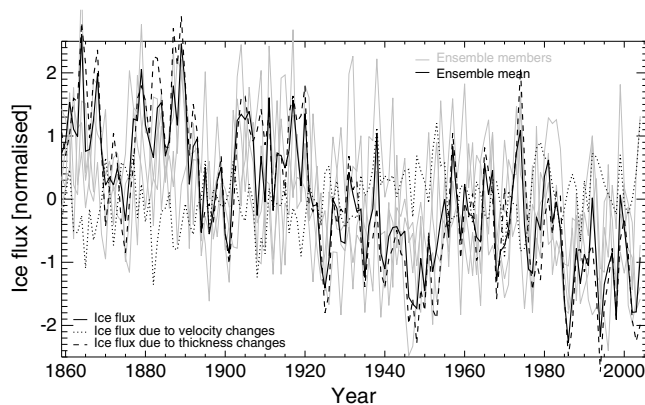


Figure 4. Normalized ice flux across 80°N in ALL (solid) ensemble mean (thick) and individual ensemble members (thin). Also plotted are ensemble mean ice flux using time-averaged thickness (to highlight velocity-driven changes, dotted), and ensemble mean ice flux using time-averaged velocity (to highlight thickness-driven changes, dashed).

further traced back to atmospheric circulation changes while mechanism (iii) appears to be an ocean circulation feedback.

[10] The reduction of the net atmosphere-to-ocean freshwater flux into the SPG in the ALL simulations is due to an increase in evaporation that is only partly offset by a corresponding increase in precipitation. The increased evaporation in ALL is associated with both increasing SSTs and changes in wind direction over the SPG. Further analysis suggests that in both ALL and ALL-AERO warming of the surface waters drives increased evaporation. However, in ALL-AERO the evaporation from surface warming is opposed by an increase in near-surface specific humidity, which is not as pronounced in ALL (not shown). This is due to the strengthening low over the SPG in ALL (Figure 6a), resulting in an increase in winds from the drier air of continental North America. Thus, although SSTs are similar in the ALL and ALL-AERO ensembles in the SPG, evaporation increases in ALL due to an increase in drier (less humid), continental air masses. There is also a small

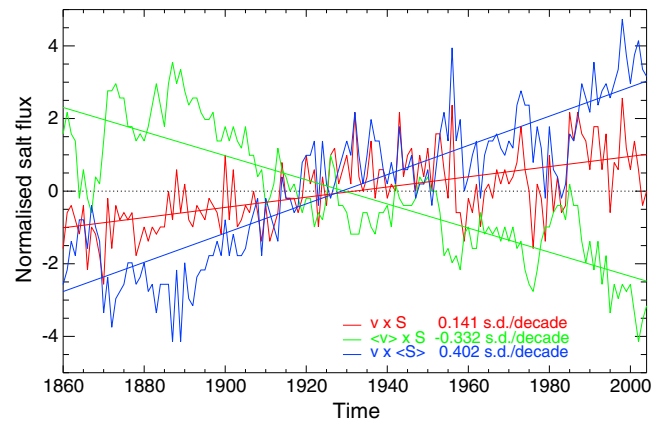


Figure 5. Annual mean normalized salt transport northward across 45°N in ALL computed using monthly mean northward velocity (v) and salinity (S) (red), time-averaged v and monthly S (to highlight salinity-driven changes, green), and time-averaged S and monthly v (to highlight velocity-driven changes, blue). All curves normalized against v times S (red). The SPG undergoes a net salinification (red line) due to increasing velocities (blue line, i.e., the AMOC), whereas the arrangement of salt within the gyre has a net freshening effect when multiplied by the velocities (green line).

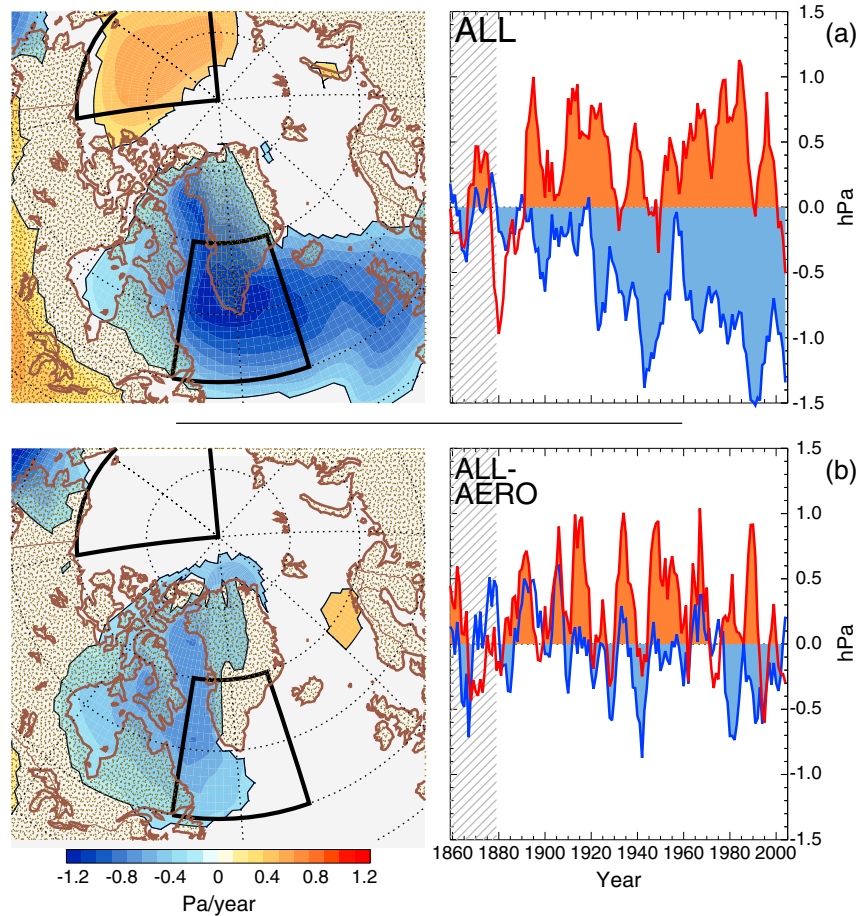


Figure 6. (left) The trend in mean sea level pressure (MSLP) in the North Atlantic/Arctic region between 1871 and 2000 for (a) ALL and (b) ALL-AEROSOL. Only data significant at the 90% level for a two-tailed t test is plotted. (right) A 5 year running mean time series of Beaufort Gyre (orange) and SPG MSLP (blue), where the regions are as indicated by the boxes on the maps.

component of the increased evaporation related to the absolute increase in wind speed but the specific humidity effect is the primary mechanism by which wind changes in this region affect the evaporation.

[11] The second process that drives salinification of the SPG in ALL is the southward transport of sea ice from the Arctic through the Fram Strait, which is reduced compared to ALL-AEROSOL. The reduction in ice volume transport is predominantly a result of thinning of sea ice in the Fram Strait region rather than changes in southward velocity (Figure 4). These changes are associated with a strengthening Beaufort Gyre in ALL, which accumulates ice and freshwater in the central Arctic with corresponding reductions farther south.

[12] Finally, the changes in ocean circulation result in a positive feedback on salt transport into the SPG. A decomposition of the advective term in the freshwater budget reveals that the changes in meridional velocities (i.e., the AMOC) in ALL are acting to salinify the SPG, whereas the changes in the salinity distribution are acting to oppose this change (Figure 5). The net result is a salinification from the advective terms.

[13] One of the main differences between ALL and ALL-AEROSOL is the atmospheric circulation, particularly in the Northern Hemisphere and North Atlantic/Arctic region. This

may be caused by differential heating of the atmosphere due to local aerosol concentrations resulting in modulation of the atmospheric circulation, although other candidates include aerosol modification of cloud lifetimes and nonlinear interactions between aerosols and other external forcings. A mechanistic analysis of the connection between aerosol forcings and atmospheric circulation will be the subject of future studies. However, we note that understanding of real-world historical aerosol emissions and forcing magnitudes is still poorly constrained, as are the representations of many aerosol processes within models [Bellouin *et al.*, 2012; Forster *et al.*, 2007]. In ALL, the key features of the mean sea level pressure (MSLP) changes are a deepening low over the SPG and an increasing high over the Beaufort Gyre (BG; Figure 6a). Such a pattern is broadly consistent with reduced Fram Strait ice export (the Arctic Dipole Anomaly) [Wu *et al.*, 2006], while the deepening SPG is consistent with increased wind speeds in this region.

[14] Regression analysis of the HadGEM2-ES control simulation provides additional evidence for a link between the SLP changes seen in ALL and the mechanisms previously discussed in section 3.2 for increasing salinity over the SPG. To perform the regression (Figure 7), decadal means of mean sea level pressure (MSLP), 0–800 m salinity, evaporation from the ocean, wind stress magnitude, and sea

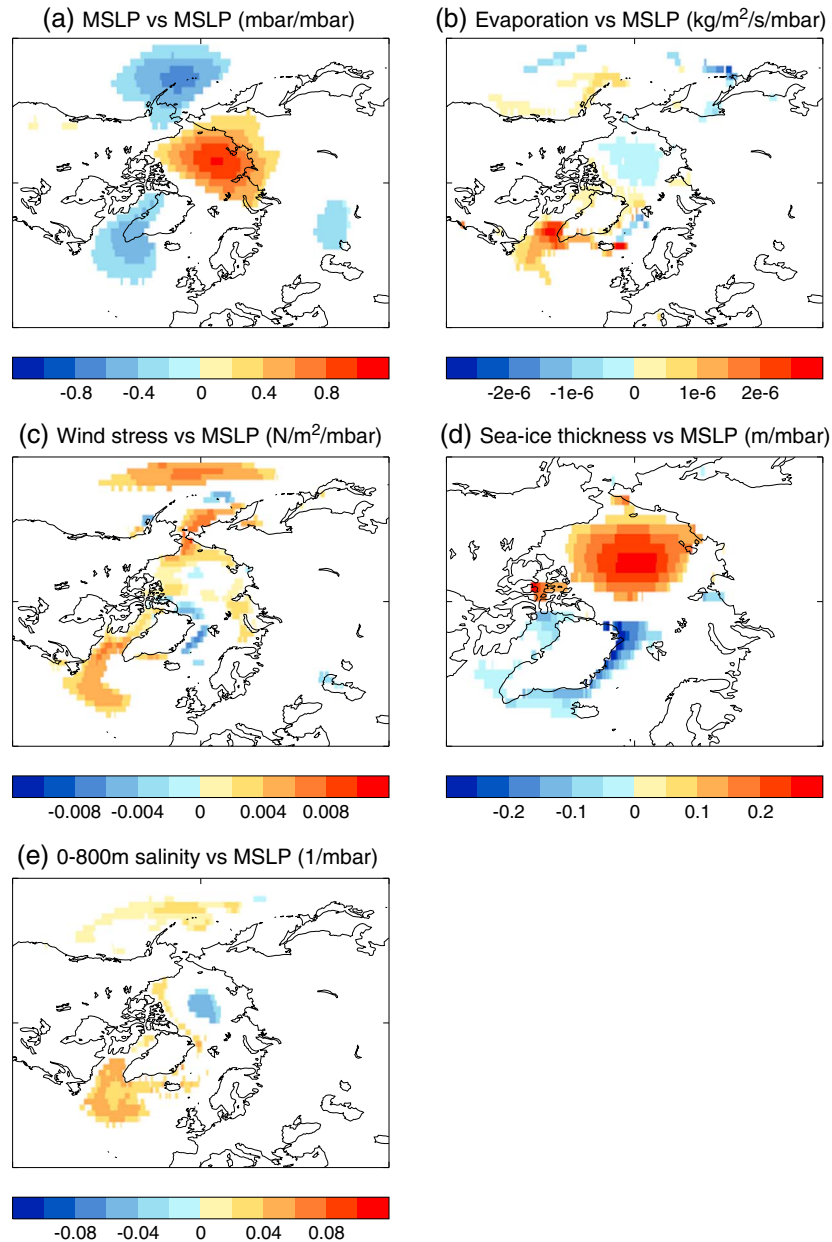


Figure 7. Decadal mean regressions in the control run between MSLP dipole index and various quantities, as described in the text. Dipole index regressed against (a) MSLP, (b) evaporation, (c) wind stress magnitude, (d) sea ice thickness, and (e) top 800 m salinity.

ice thickness were calculated from the HadGEM2-ES control simulation. A dipole index of MSLP variability was defined as the area average of decadal mean MSLP in the Beaufort Gyre (70°N–90°N, 135°E–135°W) minus the area average of decadal mean MSLP over the southern tip of Greenland (50°N–70°N, 60°W–30°W). Decadal means were used to pick out the response to sustained changes in MSLP, rather than interannual/seasonal variability. Spatial maps of linear regression coefficients were created by regressing decadal means at each point with the decadal mean MSLP dipole index. Only regression coefficients with a probability of zero correlation < 0.05 were plotted (estimated using a two-tailed t test). Thus, from Figure 7, a stronger Beaufort Gyre is associated with thicker ice and fresher conditions

in the central Arctic and thinner ice and more saline conditions farther south in the Arctic. A deepening low over the SPG is also associated with increased wind speeds and evaporation, resulting in increasing salinity.

4. Discussion

4.1. Comparison Against Reanalyses

[15] The AMOC strengthening in the ALL simulations of the coupled climate model HadGEM2-ES shows some similarities to a number of AMOC reanalyses using ocean-only models (Figure 8). In broad terms, all show a long-term increase in the AMOC, although there are differences in detail that may reflect sensitivity to initial conditions and

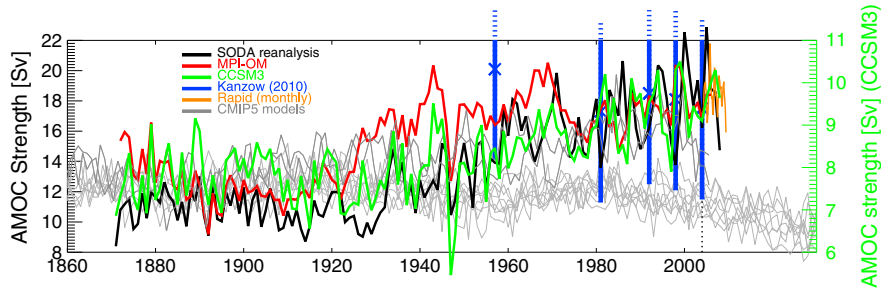


Figure 8. AMOC time series from the SODA reanalysis [Schott *et al.*, 2009] (black); the CCSM3 forced ocean model [Lee *et al.*, 2011] (green); the MPI-OM forced ocean model [Marsland *et al.*, 2003; Matei *et al.*, 2012] (red); the five hydrographic sections of Bryden *et al.* [Bryden *et al.*, 2005], as reevaluated by Kanzow *et al.* [Kanzow *et al.*, 2010], with error bars of ± 6 Sv [Ganachaud, 2003] (blue); monthly mean AMOC from the 26.5°N array [Cunningham *et al.*, 2007] (orange). Note the different scale for CCSM3. Also shown are the AMOC time series from the 14 CMIP5 models which had provided streamfunction data for the historical experiments to the CMIP5 database as of September 2012 (gray, see Table 1): CCSM4, CESM1-BGC, CESM1-CAM5, CESM1-FASTCHEM, CESM1-WACCM, CNRM-CM5, FGOALS-g2, MPI-ESM-LR, MPI-ESM-MR, MPI-ESM-P, MRI-CGCM3, NorESM1-M, NorESM1-ME, inmcm4, ACCESS1-0, ACCESS1-3. The CMIP5 models have been offset to have a mean of 12 Sv in order to compare their time evolution with the ocean model simulations and observations.

structural differences in models and data assimilation schemes. These reanalyses are all forced with the twentieth century reanalysis (20CR) [Compo *et al.*, 2011], and we note that there are some similarities between the pressure pattern in ALL (Figure 6, top) and that seen in the ensemble mean of 20CR (Figure 9), although there are limited observations in this reanalysis far back in time, which are presumably the cause of the large 20CR ensemble spread prior to the twentieth century. While tentative, the ocean reanalyses appear to provide qualitative support for the importance of this pressure pattern in affecting AMOC evolution and further investigation of the mechanisms is warranted.

[16] Time series of the AMOC from a number of other latest generation-coupled climate models available from the Coupled Model Intercomparison Project (CMIP5) database (<http://cmip-pcmdi.llnl.gov/cmip5/>; see Table 1) are also plotted and serve to highlight the continued diversity in model responses to historical forcings (Figure 8). Most models show a stable or declining AMOC during the late 19th and 20th centuries, although both ACCESS1.0 and ACCESS1.3 [Bi *et al.*, 2012] show an AMOC strengthening during this time similar in magnitude to HadGEM2-ES. The ACCESS models use a different ocean submodel to HadGEM2-ES (ACCESS1.0 incorporates the same atmospheric submodel as HadGEM2-ES while ACCESS1.3 uses

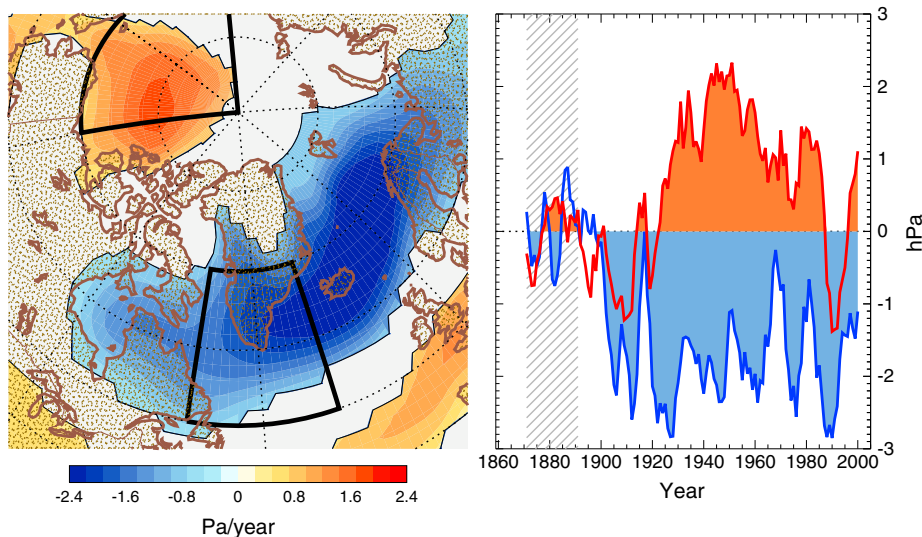


Figure 9. The trend in mean sea level pressure (MSLP) in the North Atlantic/Arctic region between 1871 and 2000 in 20CR, after Figure 6. Only data significant at the 90% level for a two-tailed *t* test is plotted. A 5 year running mean time series of Beaufort Gyre (orange) and SPG MSLP (blue), where the regions are as indicated by the boxes on the maps.

Table 1. The Modeling Groups and Models Used in Figure 8

Modeling group	Model
NCAR	CCSM4
NSF-DOE-NCAR	CESM1-BGC
NSF-DOE-NCAR	CESM1-CAM5
NSF-DOE-NCAR	CESM1-FASTCHEM
NSF-DOE-NCAR	CESM1-WACCM
CNRM-CERFACS	CNRM-CM5
LASG-CESS	FGOALS-g2
MPI	MPI-ESM-LR
MPI	MPI-ESM-MR
MPI	MPI-ESM-P
MRI	MRI-CGCM3
NCC	NorESM1-M
NCC	NorESM1-ME
INM	inmcm4
CSIRO-BOM	ACCESS1-0
CSIRO-BOM	ACCESS1-3

a similar resolution but updated dynamical core) [Bi et al., 2012], which suggests that the AMOC response is not a function of the ocean model.

[17] Arctic/North Atlantic MSLP patterns such as those in Figures 3a (for the model) and 9 (for the reanalysis) have been shown in observational studies to be related to reduced Fram Strait ice export [Proshutinsky et al., 2002; Wu et al., 2006]. Simulations of Fram Strait ice export (Figure 4) in ALL also show similar decadal variability and trends to long-term reconstructions [Schmith and Hansen, 2003] and the increase in evaporation over the SPG is qualitatively consistent with 20CR (not shown). However, key to the AMOC strengthening in ALL is the long-term salinification of the North Atlantic, most rapid between 1860 and 1930, a period which was not well observed and makes direct comparison difficult. Available observations in recent decades have shown a near-surface basin-average freshening trend

and consistent freshening signals at various deep sites in the subpolar North Atlantic [Curry and Mauritzen, 2005; Dickson et al., 2002]. However, it is also possible that this freshening is related to internal variability in the North Atlantic [Pardaens et al., 2008]. Hovmöller analysis of surface salinities shows meridionally coherent anomalies in both simulations and observations, although the magnitude of the anomalies is generally greater in the simulations (Figure 10). During the overlapping period, both simulations and observations show multiannual rather than multidecadal variability; the multidecadal salinifying trend in the simulations having all but finished by the middle of the twentieth century. These suggest that the ALL ensemble members and observation-based reconstructions show similar variability for the zonal mean surface salinity over the past few decades and highlight the sparseness of salinity observations in even the most recent years. Separately, the sea surface temperature response over the whole North Atlantic over the past 150 years compares well with observations [Booth et al., 2012], although a simulated warming trend in SST in the SPG over that time may reflect some combination of an historically incomplete observational network and/or an overestimation of the magnitude of AMOC change simulated by our model.

[18] In addition to the tantalizing similarities in the evolution of the various components of the historical AMOC strengthening mechanism between the ALL-forcings simulations with HadGEM2-ES and observation-based records/reanalyses, there are also many relevant differences: the timing and magnitudes of the AMOC strengthening in the reanalysis products is different and generally later than that in ALL (Figure 8); the surface salinity in the two observation-based data sets has a generally weaker amplitude of variability and exhibits no trend, although this would not necessarily be expected given the timing of the trends in ALL (Figure 10).

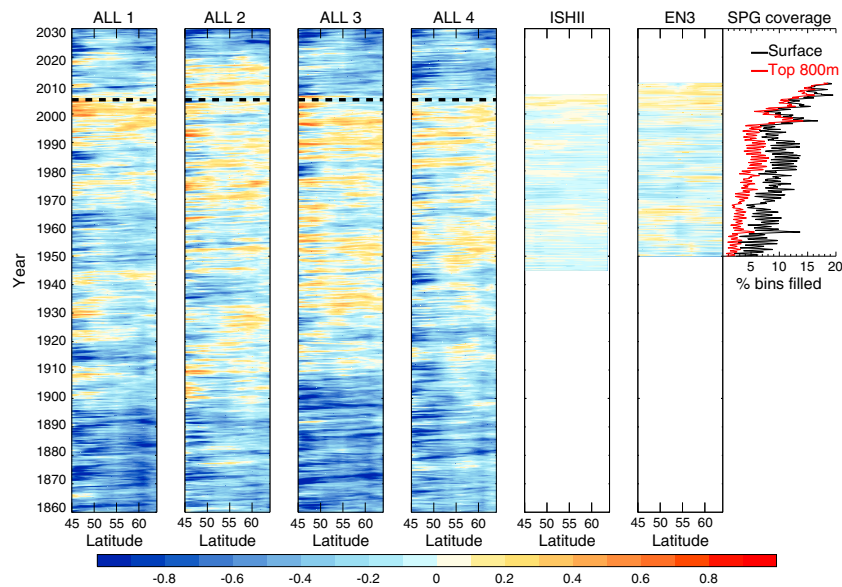


Figure 10. From left to right, deseasoned monthly zonal mean surface salinity in the North Atlantic in each of the four ALL-forcings ensemble members and the EN3 [Ingleby and Huddleston, 2007] and Ishii [Ishii et al., 2005] observational reconstructions. Also plotted on the far right is the percentage number of grid boxes in the whole North Atlantic (45°N–65°N) in EN3 filled each month with at least one observation either at the surface (black) or down to 800 m (red).

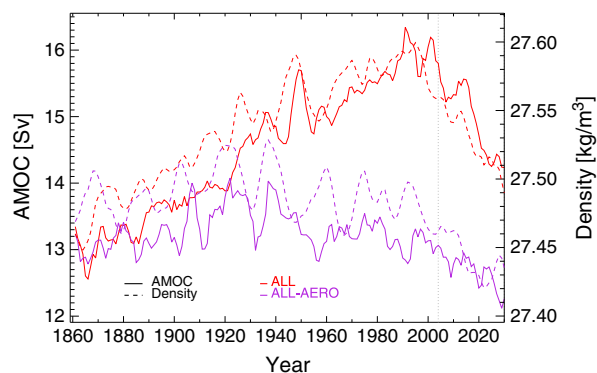


Figure 11. Five year running mean ensemble mean Labrador Sea top 800 m densities (dashed, right axis) in ALL (red) and ALL-AERO (purple). Also plotted is the ensemble mean AMOC strength in ALL and ALL-AERO (solid, left axis). Dashed gray line indicates where ensembles were switched from historical to RCP4.5 external forcings.

Additionally, many of the other CMIP5 models show no historical AMOC strengthening (Figure 8), similar to results from previous coupled climate models [Meehl *et al.*, 2007]. In HadGEM2-ES, it is clear that aerosol forcing plays a key climate role, perhaps more so than in other models, and that this forcing is still uncertain [Bellouin *et al.*, 2012]. It is possible that aerosol forcing is stronger in HadGEM2-ES than in reality, although we note that it is not an outlier within the multimodel ensemble in terms of the direct and indirect effects of aerosols [Quaas, 2009]. Whether the differences between HadGEM2-ES (and the ACCESS models) and other members of the CMIP5 archive reflect deficiencies in the former or latter, or some combination thereof, is unclear. In either case, understanding of the mechanisms causing the modeled AMOC strengthening is important and raises further questions. For example, what does an historical strengthening driven by aerosols imply for the present-day and future evolution of the AMOC in our model?

4.2. Future Changes

[19] From 2005 to 2030, we extend the ALL simulations following the CMIP5 RCP4.5 forcing scenario [Moss *et al.*, 2010], which includes a continued reduction in aerosol forcing (Figure 1b). During this period, there is subpolar freshening due to increasing ice melt as well as a reduction in the salinification mechanism due to decreased aerosol emissions. This freshening reinforces the warming-driven density changes due to increasing greenhouse gases, leading to decreased SPG density (Figure 2a), and rapid weakening of the AMOC (Figure 1a). Between 2010 and 2030, the rate of AMOC weakening in ALL is 3 times larger than in other simulations (ALL-AERO) where anthropogenic aerosol emissions are held constant at preindustrial values, although the AMOC is still stronger in 2030 in ALL than in ALL-AERO. The increased rate of weakening in ALL compared to ALL-AERO occurs despite a similar trend in SPG anomalous density from the year 2000 (Figures 2a and 2b). This suggests a change in the relationship between SPG density and the AMOC during the 21st century. Further analysis indicates that changes at the gyre boundaries and in the Labrador Sea are increasingly decoupled from changes in the centre of

the gyre. When we restrict our analysis to the Labrador Sea (55°N–65°N, 45°W–60°W), the strength of the AMOC and the top 800 m density are strongly correlated throughout the simulations (Figure 11). This result emphasises the importance of the Labrador Sea as a location for deepwater formation and open ocean convection and illustrates the potential for changes in the relationship between near-surface densities in the Labrador Sea and the wider SPG. Thus, the sensitivity of the AMOC to aerosol forcing has potential implications for the future evolution of the AMOC in HadGEM2-ES. This underlines the importance of understanding the base climate and sensitivities of any model which may be used as the basis for decadal predictions.

5. Conclusions

[20] We have reported the potential importance of aerosol forcing since 1860 on the AMOC and explored the key mechanisms of ocean response in HadGEM2-ES. These mechanisms are (i) a decrease in ice transport through the Fram Straits, (ii) increased evaporation in the SPG, and (iii) a positive ocean circulation feedback. All of these effects act to salinify the North Atlantic in our model resulting in a decrease in stability of the water column, increased convection, and an increase in strength of the AMOC. These changes are all ultimately related to simulated MSLP changes over the Arctic and North Atlantic.

[21] Analysis of the CMIP5 archive suggests most models do not show an historically strengthening AMOC highlighting the continued and possible increase in the diversity of model responses to external forcings. It is also intriguing that a number of ocean-only simulations are in qualitative agreement with the ALL simulations. However, due to the lack of long-term measurement of the AMOC, we cannot rule out the possibility that the strengthened AMOC in ALL is the result of an incomplete understanding and implementation of aerosol processes. This again emphasizes the importance of sustained direct observations of the AMOC, such as the RAPID array, for constraining model-based understanding of this important phenomenon. Nevertheless, if anthropogenic aerosols have indeed contributed to a strengthening of the AMOC over the twentieth century, then it should be highlighted that future reductions in aerosol emissions may compound the projected weakening associated with GHG forcing over the coming decades.

[22] **Acknowledgments.** The research leading to these results has received funding from the European Community's seventh framework programme (FP7/2007-2013) under grant agreement no. GA212643 (THOR: "Thermohaline Overturning – at Risk," 2008–2012) and was supported by the Joint DECC and Defra Hadley Centre Climate Programme, DECC/Defra (GA01101) and the UK Natural Environment Research Council. The HadGEM2-ES data are available on the CMIP5 model archive at <http://pcmdi3.llnl.gov/esgcat/home.htm>. The authors would like to thank John Hughes for setting up the HadGEM2-ES ALL experiments.

References

- Bellouin, N., G. W. Mann, M. T. Woodhouse, C. Johnson, K. S. Carslaw, and M. Dalvi (2012), Impact of the modal aerosol scheme GLOMAP-mode on aerosol forcing in the Hadley Centre Global Environmental Model, *Atmos. Chem. Phys. Discuss.*, 12(8), 21437–21479.
- Bi, D., *et al.* (2012), The ACCESS coupled model: Description, control climate and evaluation, *Aust. Meteorol. Oceanogr. J.*, in press.
- Booth, B. B. B., N. J. Dunstone, P. R. Halloran, T. Andrews, and N. Bellouin (2012), Aerosols implicated as a prime driver of twentieth-century North

- Atlantic climate variability (vol 484, pg 228, 2012), *Nature*, 485(7399), 534–534.
- Bryden, H. L., H. R. Longworth, and S. A. Cunningham (2005), Slowing of the Atlantic meridional overturning circulation at 25 degrees N, *Nature*, 438(7068), 655–657.
- Cai, W., D. Bi, J. Church, T. Cowan, M. Dix, and L. Rotstayn (2006), Pan-oceanic response to increasing anthropogenic aerosols: Impacts on the Southern Hemisphere oceanic circulation, *Geophys. Res. Lett.*, 33, L21707, doi:10.1029/2006GL027513.
- Clark, P. U., N. G. Pisias, T. F. Stocker, and A. J. Weaver (2002), The role of the thermohaline circulation in abrupt climate change, *Nature*, 415(6874), 863–869.
- Collins, W. J., et al. (2011), Development and evaluation of an Earth-system model—HadGEM2, *Geoscientific Model Dev*, doi:10.5194/gmdd-4-997-2011.
- Compo, G. P., et al. (2011), The twentieth century reanalysis project, *Q. J. R. Meteorol. Soc.*, 137(654), 1–28.
- Cunningham, S. A., et al. (2007), Temporal variability of the Atlantic meridional overturning circulation at 26.5 degrees N, *Science*, 317(5840), 935–938.
- Curry, R., and C. Mauritzen (2005), Dilution of the northern North Atlantic Ocean in recent decades, *Science*, 308(5729), 1772–1774.
- Delworth, T. L., and K. W. Dixon (2006), Have anthropogenic aerosols delayed a greenhouse gas-induced weakening of the North Atlantic thermohaline circulation?, *Geophys. Res. Lett.*, 33, L02606, doi:10.1029/2005GL024980.
- Dickson, B., I. Yashayaev, J. Meincke, B. Turrell, S. Dye, and J. Holford (2002), Rapid freshening of the deep North Atlantic Ocean over the past four decades, *Nature*, 416(6883), 832–837.
- Forster, P., et al. (2007), Chapter 2: Changes in Atmospheric Constituents and Radiative Forcing, in *Climate Change 2007: the Physical Science Basis*. Contribution of WGI to the Fourth Assessment Report of the IPCC, Cambridge University Press, Cambridge.
- Ganachaud, A. (2003), Error budget of inverse box models: The North Atlantic, *J. Atmos. Ocean Technol.*, 20(11), 1641–1655.
- Gregory, J. M., et al. (2005), A model intercomparison of changes in the Atlantic thermohaline circulation in response to increasing atmospheric CO₂ concentration, *Geophys. Res. Lett.*, 32, L02606, doi:10.1029/2005GL024980.
- Ingleby, B., and M. Huddleston (2007), Quality control of ocean temperature and salinity profiles—Historical and real-time data, *J. Mar. Syst.*, 65(1–4), 158–175.
- Ishii, M., A. Shouji, S. Sugimoto, and T. Matsumoto (2005), Objective analyses of sea-surface temperature and marine meteorological variables for the 20th century using ICOADS and the Kobe collection, *Int. J. Climatol.*, 25(7), 865–879.
- Johns, W. E., et al. (2011), Continuous, array-based estimates of Atlantic ocean heat transport at 26.5 degrees N, *J. Clim.*, 24(10), 2429–2449.
- Jones, C. D., et al. (2011), The HadGEM2-ES implementation of CMIP5 centennial simulations, *Geoscientific Model Dev*, doi:10.5194/gmd-4-543-2011.
- Kanzow, T., et al. (2010), Seasonal variability of the Atlantic meridional overturning circulation at 26.5 degrees N, *J. Clim.*, 23(21), 5678–5698.
- Latif, M., and N. S. Keenlyside (2011), A perspective on decadal climate variability and predictability, *Deep-Sea Res II*, 58(17–18), 1880–1894.
- Lee, S. K., W. Park, E. van Sebille, M. O. Baringer, C. Z. Wang, D. B. Enfield, S. G. Yeager, and B. P. Kirtman (2011), What caused the significant increase in Atlantic Ocean heat content since the mid-20th century?, *Geophys. Res. Lett.*, 38, L17607, doi:10.1029/2011GL048856.
- Marsland, S. J., H. Haak, J. H. Jungclauss, M. Latif, and F. Roske (2003), The Max-Planck-Institute global ocean/sea ice model with orthogonal curvilinear coordinates, *Ocean Model*, 5(2), 91–127.
- Matei, D., H. Pohlmann, J. Jungclauss, W. A. Muller, H. Haak, and J. Marotzke (2012), Two tales of initializing decadal climate predictions experiments with the ECHAM5/MPI-OM model, *J. Clim.*, 25(24), 8502–8523.
- McManus, J. F., R. Francois, J. M. Gherardi, L. D. Keigwin, and S. Brown-Leger (2004), Collapse and rapid resumption of Atlantic meridional circulation linked to deglacial climate changes, *Nature*, 428(6985), 834–837.
- Meehl, G. A., et al. (2007), Chapter 10: Global Climate Projections, in *Climate Change 2007: the Physical Science Basis*. Contribution of WGI to the Fourth Assessment Report of the IPCC, Cambridge University Press, Cambridge.
- Minobe, S., A. Kuwano-Yoshida, N. Komori, S. P. Xie, and R. J. Small (2008), Influence of the Gulf Stream on the troposphere, *Nature*, 452(7184), 206–U251.
- Moss, R. H., et al. (2010), The next generation of scenarios for climate change research and assessment, *Nature*, 463(7282), 747–756.
- Pardaens, A., M. Vellinga, P. Wu, and B. Ingleby (2008), Large-scale Atlantic salinity changes over the last half-century: A model-observation comparison, *J. Clim.*, 21(8), 1698–1720.
- Proshutinsky, A., R. H. Bourke, and F. A. McLaughlin (2002), The role of the Beaufort Gyre in Arctic climate variability: Seasonal to decadal climate scales, *Geophys. Res. Lett.*, 29(23), 2100, doi:10.1029/2002GL015847.
- Quaas, J., Y. Ming, S. Menon, T. Takemura, M. Wang, J. E. Penne, and M. Schulz (2009), Aerosol indirect effects-general circulation model intercomparison and evaluation with satellite data, *Atmos. Chem. Phys.*, 9(22), 8697–8717.
- Schmith, T., and C. Hansen (2003), Fram Strait ice export during the nineteenth and twentieth centuries reconstructed from a multiyear sea ice index from southwestern Greenland, *J. Clim.*, 16(16), 2782–2791.
- Schmittner, A., M. Latif, and B. Schneider (2005), Model projections of the North Atlantic thermohaline circulation for the 21st century assessed by observations, *Geophys. Res. Lett.*, 32, L23710, doi:10.1029/2005GL024368.
- Schott, F. A., L. Stramma, B. S. Giese, and R. Zantopp (2009), Labrador Sea convection and subpolar North Atlantic Deep Water export in the SODA assimilation model, *Deep-Sea Res I*, 56(6), 926–938.
- Stouffer, R. J., et al. (2006), Investigating the causes of the response of the thermohaline circulation to past and future climate changes, *J. Clim.*, 19(8), 1365–1387.
- Thorpe, R. B., J. M. Gregory, T. C. Johns, R. A. Wood, and J. F. B. Mitchell (2001), Mechanisms determining the Atlantic thermohaline circulation response to greenhouse gas forcing in a non-flux-adjusted coupled climate model, *J. Clim.*, 14(14), 3102–3116.
- Vellinga, M., and R. A. Wood (2002), Global climatic impacts of a collapse of the Atlantic thermohaline circulation, *Clim. Chang.*, 54(3), 251–267.
- Wu, B. Y., J. Wang, and J. E. Walsh (2006), Dipole anomaly in the winter Arctic atmosphere and its association with sea ice motion, *J. Clim.*, 19(2), 210–225.
- Zhang, R., and T. L. Delworth (2005), Simulated tropical response to a substantial weakening of the Atlantic thermohaline circulation, *J. Clim.*, 18(12), 1853–1860.